Electronic Supplementary Information

Enhanced Water Transportation on a Superhydrophilic Serial Cycloid-Shaped Pattern

Defeng Yan[1], Yi Lu[1], Jinming Liu[1], Yang Chen[1], Jing Sun[1], and Jinlong Song[1, 2]*

1 State Key Laboratory of High-performance Precision Manufacturing, Dalian University of Technology, Dalian Liaoning, 116024, China.
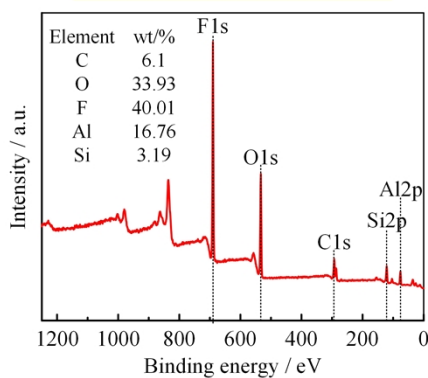
2 Key Laboratory for Micro/Nano Technology and System of Liaoning Province, Dalian University of Technology, Dalian Liaoning, 116024, China.

*Corresponding author: songjinlong@dlut.edu.cn
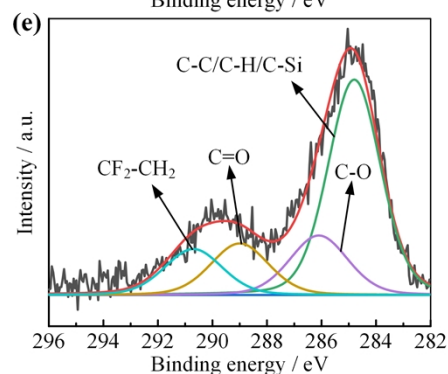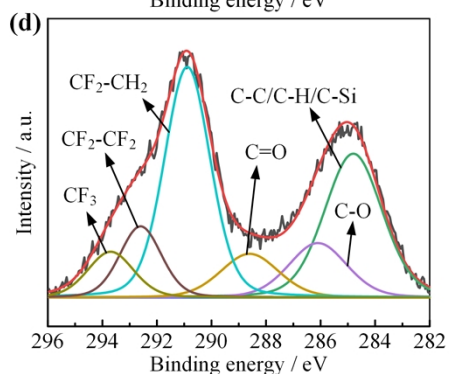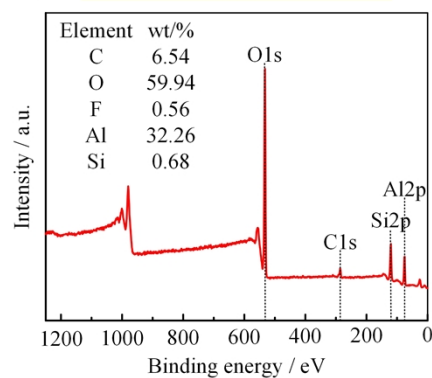
● **Figures**
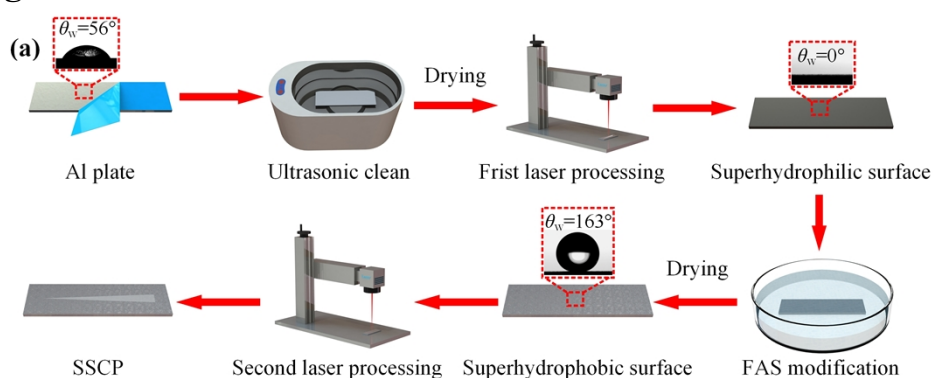
Figure S1. Schematics of the fabrication processes and X-Ray Photoelectron Spectroscopy (XPS)

spectra. (a) Schematics of the fabrication processes of the superhydrophilic serial cycloid-shaped pattern (SSCP). (b) XPS spectra of the superhydrophobic surface. The Fluoroalkylsilane (FAS) was modified to the Al plate which obtained superhydrophobicity. (c) XPS spectra of the SSCP. The second laser processing removed the most of the FAS layer, causing that the SSCP obtained superhydrophilicity. (d) Peak-fitted high-resolution C 1s XPS spectra of the superhydrophobic surface. (e) Peak-fitted high-resolution C 1s XPS spectra of the SSCP. θ_w means the water contact angle.
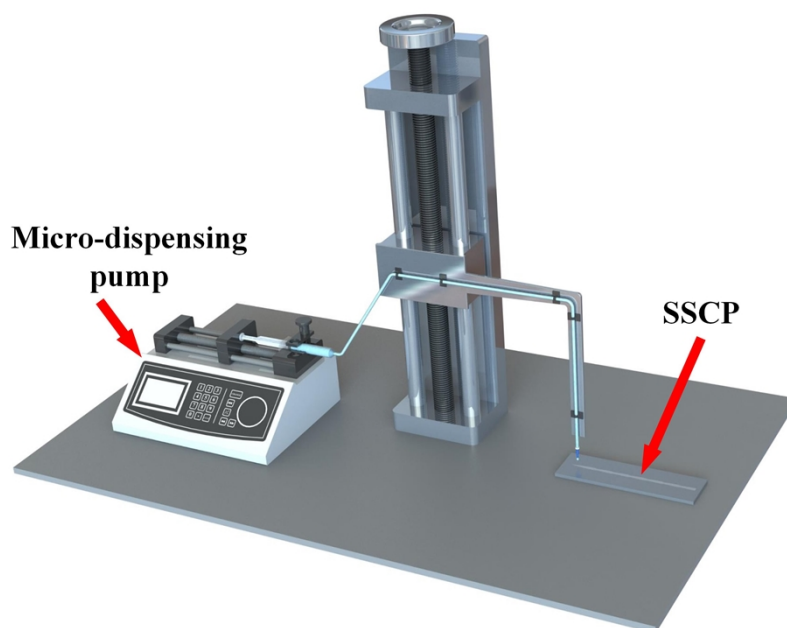
Figure S2. Schematics of the water transportation test equipment.
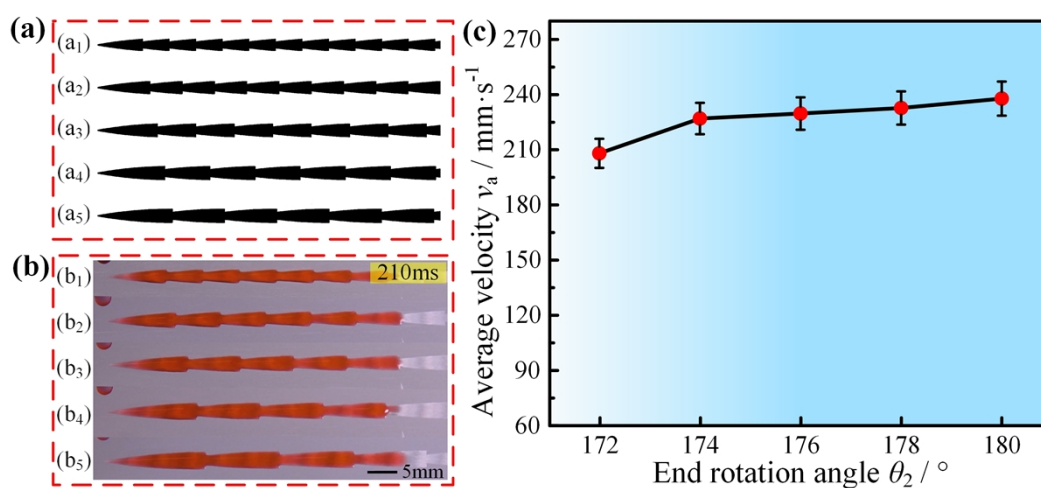

Figure S3. The influence of the end rotation angle θ_2 on the water transportation velocity by the single-factor experiment. (a) Schematic of the SSCP with the different end rotation angles. (b, c) The transportation processes and the average water transportation velocity of a 40 μL water droplet on the SSCP with the different end rotation angles.
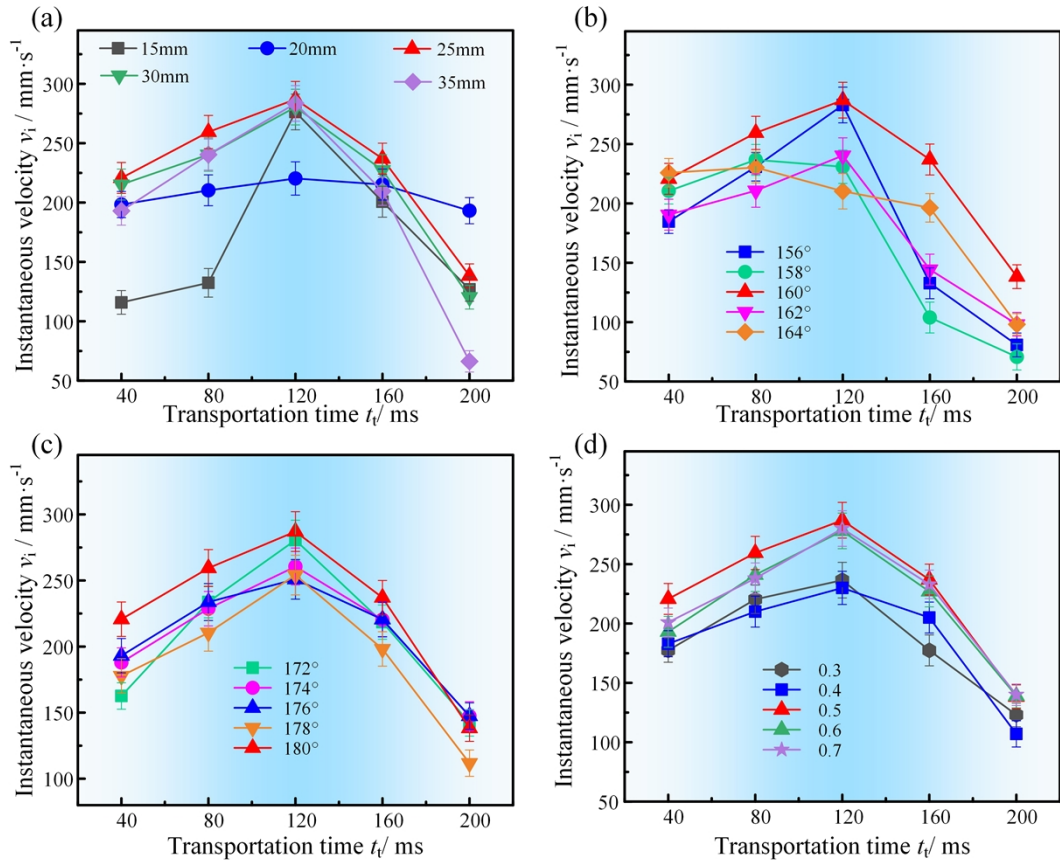
Figure S4. The influence of the SSCP parameters on the instantaneous velocity by the single-factor experiments. (a) The instantaneous velocity of a 40 μL water droplet on the SSCP with the different rolling circle radii. (b) The instantaneous velocity of a 40 μL water droplet on the SSCP with the different start rotation angles. (c) The instantaneous velocity of a 40 μL water droplet on the SSCP with the different end rotation angles. (d) The instantaneous velocity of a 40 μL water droplet on the SSCP with the different ratios of the narrow width to the wide width.
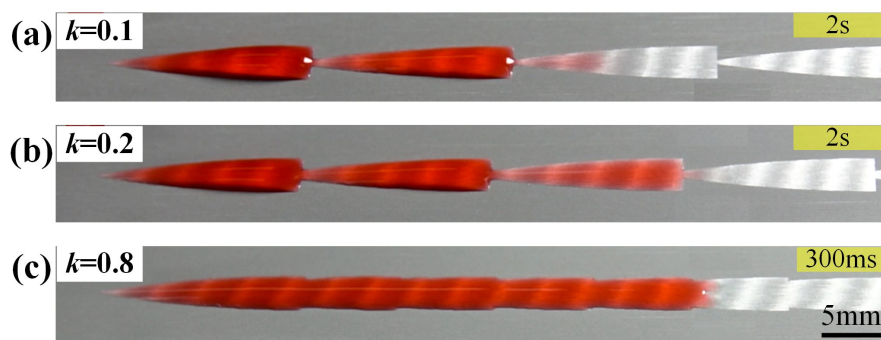
Figure S5. The transportation processes of the water droplet on the SSCP with the different ratios of the narrow width to the wide width k. (a) The image of a 40 μL water droplet on the SSCP with the k=0.1 after 2 s. (b) The image of a 40 μL water droplet on the SSCP with the k=0.2 after 2 s. The water droplet would be blocked at the junction when the k <0.3. (c) The image of a 40 μL water droplet on the SSCP with the k=0.8 after 300 ms.
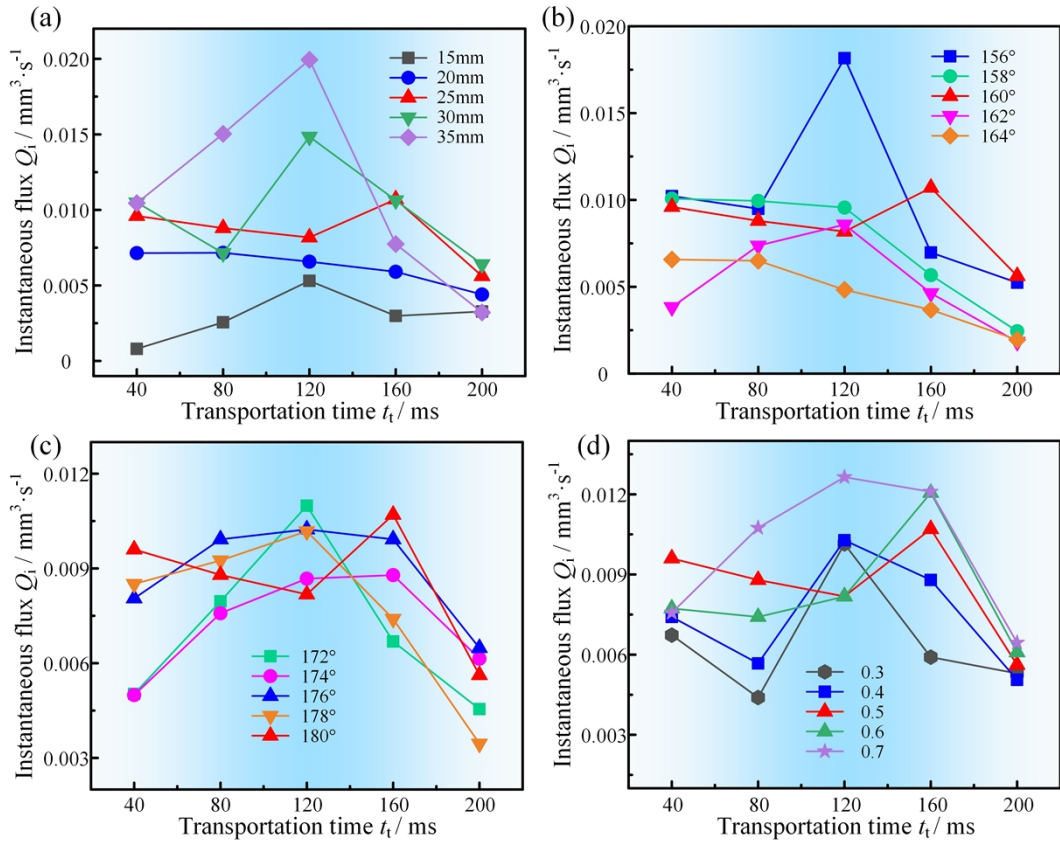
Figure S6. The influence of the SSCP parameters on the instantaneous water transportation flux by the single-factor experiments. (a) The instantaneous water transportation flux of a 40 μL water droplet on the SSCP with the different rolling circle radii. (b) The instantaneous water transportation flux of a 40 μL water droplet on the SSCP with the different start rotation angles. (c) The instantaneous water transportation flux of a 40 μL water droplet on the SSCP with the different end rotation angles. (d) The instantaneous water transportation flux of a 40 μL water droplet on the SSCP with the different ratios of the narrow width to the wide width.
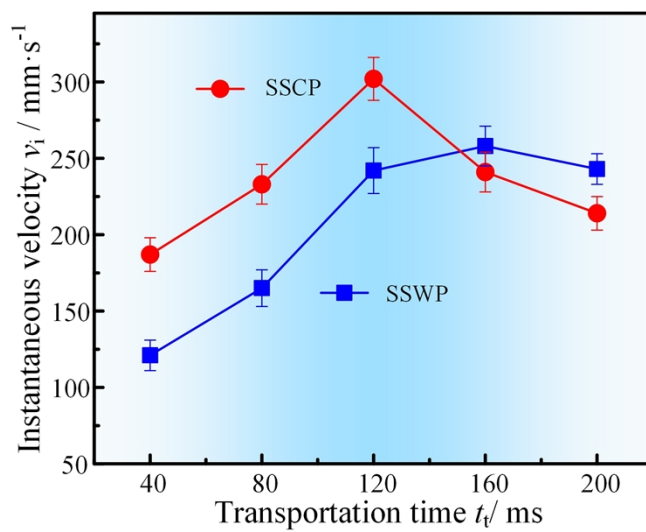

Figure S7. The instantaneous velocity of water droplet on the SSCP and the SSWP.
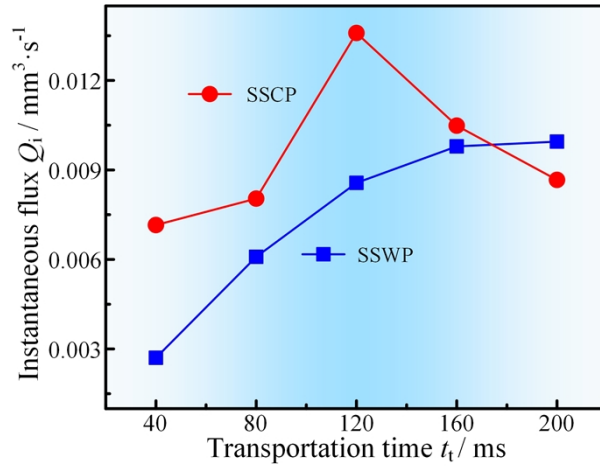
Figure S8. The instantaneous water transportation flux of water droplet on the SSCP and the SSWP.
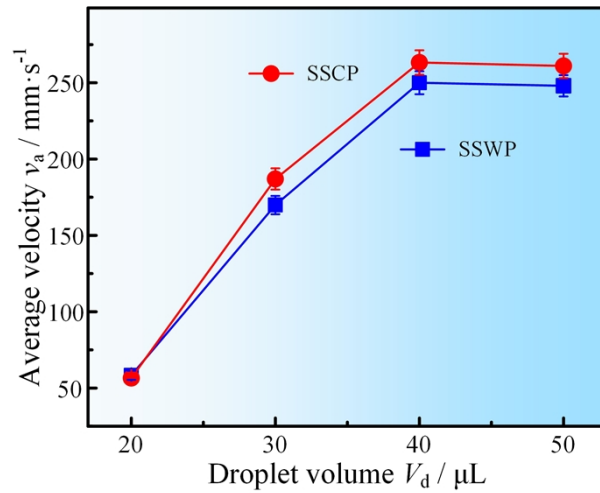
Figure S9. The average water transportation velocity of different droplet volumes on the SSWP and the SSCP.
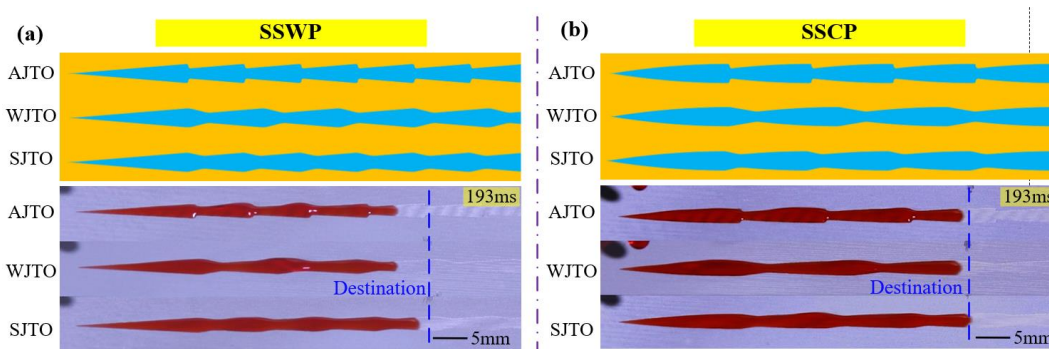
Figure S10. The schematics and images of the SSWP and the SSCP after the junction optimization. (a) The schematics and optical images of the SSWP after the arc junction transition optimization (SSWP$_{AJTO}$), wedge junction transition optimization (SSWP$_{WJTO}$), and streamline junction transition optimization (SSWP$_{SJTO}$). (b) The schematics and optical images of the SSCP after the arc junction transition optimization (SSCP$_{AJTO}$), wedge junction transition optimization (SSCP$_{WJTO}$), and streamline junction transition optimization (SSCP$_{SJTO}$).
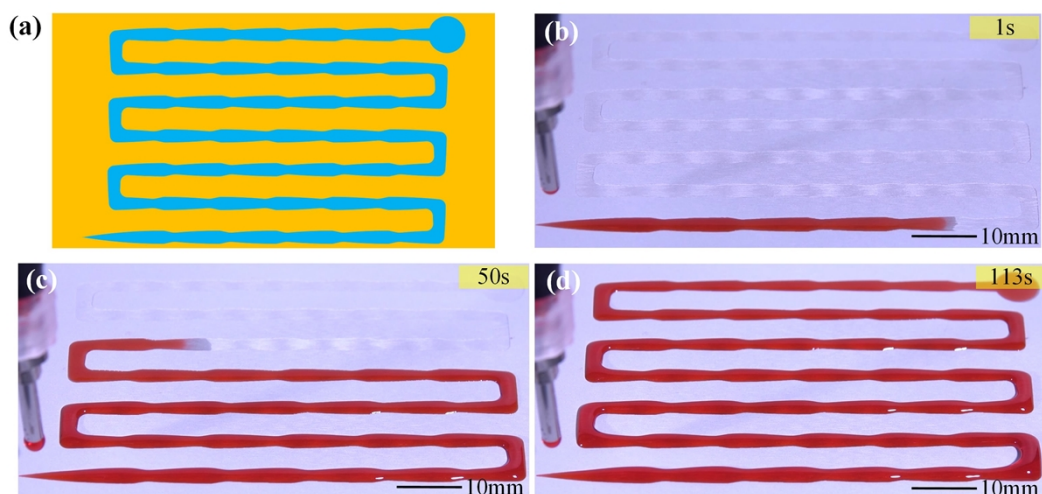
Figure S11. Schematic of the long-distance SSCP and the digital images of the water transportation process on the long-distance SSCP pattern. (a) Schematic of the long-distance SSCP with ~53 cm. (b-d) The transportation processes of the water on the long-distance SSCP with ~53 cm.

Figure S12. The optical images of the entire superhydrophilic surface (SHI), entire superhydrophobic surface (SHP), superhydrophilic single wedge-shaped pattern (SWP), superhydrophilic serial wedge-shaped pattern (SSWP), and superhydrophilic serial cycloid-shaped pattern (SSCP).

Tables

Table S1 The variance analysis of the experimental results

Source of variance	Sum of squares	Degree of freedom	Mean squares	F value	P value
Model	20162.23	9	2240.25	32.27	<0.0001**
r	1090.58	1	1090.58	15.71	0.0016**
θ_1	870.06	1	870.06	12.53	0.0036**
k	7965.26	1	7965.26	114.75	<0.0001**
$r \cdot \theta_1$	589.62	1	589.62	8.49	0.0121*
$r \cdot k$	717.07	1	717.07	10.33	0.0068**
$k \cdot \theta_1$	2.58	1	2.58	0.037	0.8502
r^2	1580.99	1	1580.99	22.78	0.0004**
θ_1^2	841.52	1	841.52	12.12	0.0041**
k^2	6555.46	1	6555.46	94.44	<0.0001**
Residual error	902.41	13	69.42		
Lack of fit	528.16	5	105.63	2.26	0.1464
Error	374.26	8	46.78		
Total	21064.65	22			

Note：$P \leq 0.01$ means highly significant (**); $0.01 \leq P \leq 0.05$ means significant (*); $P \geq 0.05$ means insignificant.

Table S2 The ANOVA after removing the insignificant factor

Source of variance	Sum of	Degree of	Mean	F value	P value
Model	20159.66	8	2519.957	38.98321	<0.0001**
r	1090.581	1	1090.581	16.87105	0.0011**
θ_1	870.0644	1	870.0644	13.45972	0.0025**
k	7965.264	1	7965.264	123.221	<0.0001**
$r \cdot \theta_1$	589.6178	1	589.6178	9.121264	0.0092**
$r \cdot k$	717.0685	1	717.0685	11.0929	0.0050**
r^2	1580.991	1	1580.991	24.45759	0.0002**
θ_1^2	841.5193	1	841.5193	13.01813	0.0029**
k^2	6555.458	1	6555.458	101.4116	<0.0001**
Residual error	904.9896	14	64.64211		
Lack of fit	530.7342	6	88.4557	1.890809	0.1985
Error	374.2554	8	46.78193		
Total	21064.65	22			

Note：$P \leq 0.01$ means highly significant (**); $0.01 \leq P \leq 0.05$ means significant (*); $P \geq 0.05$ means insignificant.

● **Videos**

Video S1. The transportation processes of the 40 μL water droplet on the SSWP and the SSCP. The parameter configuration of the SSWP is the first unit pattern length of 22.9 mm, wide side width of 2 mm, and narrow side width of 1.2 mm. The parameter configuration of the SSCP is the wedge angle of 5°, wide side width of 2 mm, and narrow side width of 1.2 mm.

Video S2. The influences of the SSCP parameters on the water transportation. The SSCP parameters include the rolling circle radius, start rotation angle, end rotation angle, and ratio of the narrow width to the wide width.

Video S3. The transportation processes of the 40 μL water droplet on the SSCP after the orthogonal optimization design and the SSWP with the same first unit pattern length, wide side width, and narrow side width.

Video S4. The transportation processes of the 40 μL water droplet on the SSWP and the SSCP with the arc junction transition optimization, wedge junction transition optimization, and streamline junction transition optimization.

Video S5. The influences of the prewetting SSCP on the water transportation.

Video S6. The transportation processes of the water on the long-distance SSCPs with ~23 cm and ~53 cm.

Video S7. The transportation process of the water on the SSCP with inclined angle of 6°.

Video S8. The fog collection processes of the SSCP.